Zeitschrift: Helvetica Physica Acta
Band: 58 (1985)
Heft: 4

Artikel: Fourier transform of momentum distribution in vanadium
Autor: Singh, A.K. / Manuel, A.A. / Singru, R.M.
DOI: https://doi.org/10.5169/seals-115623

Helvetica Physica Acta, Vol. **58** (1985) 640–656 0018–0238/85/040640–17$1.50 + 0.20/0

Fourier transform of momentum distribution in vanadium

By A. K. Singh, A. A. Manuel, R. M. Singru*) and M. Peter, Département de Physique de la Matière Condensée, Université de Genève, CH-1211 Genève-4, Switzerland.

(2. X. 1984)

Abstract. Experimental Compton profile (CP) and 2D-angular correlation of positron annihilation radiation (2γ) data from vanadium are analyzed by the mean of their Fourier transform $B^{CP}(\vec{r})$ and $B^{2\gamma}(\vec{r})$. They are compared with the $B^{CP}(\vec{r})$ and $B^{2\gamma}(\vec{r})$ functions calculated with the help of both the linear muffin-tin orbital and the Hubbard–Mijnarends band structure methods. The results show that the $B(\vec{r})$ functions are influenced by the positron wave function, by the $e^+ - e^-$ many-body correlations and by the differences in the electron wave functions used for the band structure calculations. We observe that $B(\vec{r})$ has an anisotropic behaviour characterized by peaks localized at the positions of the lattice translations vectors. This is in good agreement with the established properties of the $B(\vec{r})$ function. We conclude that Fourier analysis is a sensitive approach to investigate the momentum distributions in transition metals and to understand the effects of the positron.

1. Introduction

Momentum distributions of electrons in solids can be experimentally determined either by measuring Compton profiles (CP) [1] or the angular correlation of positron annihilation radiation (ACPAR) [2, 3]. The experimental results obtained by these two techniques may be compared with theoretical band structure calculations in the momentum space by using different approaches [4]. Recent work has shown that the Fourier transform of the momentum distributions (FTMD), $B(\vec{r})$, which is also called the reciprocal form factor, provide an interesting and useful approach through which the directional CP and ACPAR data can be analyzed [3, 5–12]. Such an analysis is particularly valuable for transition metals whose electron momentum distribution (EMD) and Fermi surface (FS) are not yet completely understood.

The momentum distribution in V has already been studied both experimentally and theoretically by various workers (see references cited in [9], [13] and [15]) to determine its interesting band structure and FS. It is also well known that the band structure and FS of other group VB metals, Nb and Ta, are similar to that of V. Among the transition metals, the FTMD for V [9, 10], Fe [11] and Cu [12] have been obtained from the experimental and theoretical CP data. These studies have provided a valuable comparison between the experiment and theory. However, calculations of FTMD for a transition metal using ACPAR data have not

*) Department of Physics, Indian Institute of Technology, Kanpur-208016, India.

been reported so far. Ideally a complete study should, for a given metal, compare the FTMD obtained from experimental CP and ACPAR data with the FTMD obtained from theoretical CP and ACPAR results calculated using the *same* set of electron wave functions. We report here such a systematic analysis of the FTMD for metallic V using (i) the experimental CP [9] and two-dimensional (2D) ACPAR data [13] and (ii) the theoretical EMD results for CP calculated by the linear muffin-tin orbitals (LMTO) method [14] and the theoretical momentum density for ACPAR results calculated by a) LMTO method [14] and b) Hubbard–Mijnarends method [18]. We are not aware of previous Fourier analyses for 2D-ACPAR data in a 3d metal. A comparison of the various FTMD obtained has been carried out to examine the effects of positron wave function and e^+-e^- many-body correlations [2] on the $B(\vec{r})$ function.

The scope of the paper is as follow. In Section 2, we give the basic relations used in the Fourier analysis of the momentum distribution. We put the emphasis on the differences between Compton profiles and positron annihilation distributions. In Section 3, we describe how the various $B(\vec{r})$ functions were calculated from experimental data and from band structure calculations. The Section 4 is devoted to the results we have obtained. We present various sets of $B(\vec{r})$ functions and discuss their shape and amplitudes. Finally, in Section 5, we give the conclusions drawn from this work.

2. Theory

The FTMD is described through the function $B(\vec{r})$, which was first introduced by Benesch et al. [16]. We outline below the formalism of FTMD by following the notation used by Berko [3]. The function $B(\vec{r})$, is defined [5–8] as

$$B(\vec{r}) = (2\pi)^{-3/2} \int_{-\infty}^{\infty} \exp[-i\vec{p}\cdot\vec{r}]\rho(\vec{p})\, d\vec{p}$$
$$= \mathrm{FT}_{-3}\{\rho(\vec{p})\} \tag{1}$$

where $\rho(\vec{p})$ is the electron momentum distribution. Since the CP, $J(p_z)$, is related to the EMD, $\rho(\vec{p})$, through the relation

$$J(p_z) = \text{Const.} \int_{-\infty}^{\infty} \int_{-\infty}^{\infty} \rho(\vec{p})\, dp_x\, dp_y \tag{2}$$

we have

$$B(0, 0, z) = (2\pi)^{-1/2}\mathrm{FT}_{-1}\{J(p_z)\} \tag{3}$$

The measurements of ACPAR are determined by the two-photon momentum distribution (TPMD) [2, 3], $\rho^{2\gamma}(\vec{p})$, and one can define [3] a corresponding quantity $B^{2\gamma}(\vec{r})$ as

$$B^{2\gamma}(\vec{r}) = \mathrm{FT}_{-3}\{\rho^{2\gamma}(p)\} \tag{4}$$

The measured 2D-ACPAR surfaces, $N(p_y, p_z)$, can thus be Fourier-transformed [3] to obtain

$$B^{2\gamma}(0, y, z) = (2\pi)^{-1}\mathrm{FT}_{-2}\{N(p_y, p_z)\} \tag{5}$$

It is thus seen that the FTMD of the CP data provide one component of the total $B(\vec{r})$ while that of the 2D-ACPAR data provide two components of the total $B^{2\gamma}(\vec{r})$. We shall now denote by $B^{CP}(\vec{r})$ the $B(\vec{r})$ function obtained from the CP data.

It can be shown [5–8] that in the independent particle model (IPM), $B^{CP}(\vec{r})$ is the autocorrelation function of the electron wave functions in the real space, i.e.

$$B^{CP}(\vec{r}) = \sum_j \int \psi_j^*(\vec{r}+\vec{s})\psi_j(\vec{s})\, d\vec{s} \tag{6}$$

where $\psi_j(\vec{r})$ is the $\vec{r}$-space electron wave function. On the other hand, $B^{2\gamma}(\vec{r})$, the FTMD obtained from the ACPAR data, is an autocorrelation function of $[\psi_+(\vec{r})\psi_j(\vec{r})]$, the product of the positron wave function, $\psi_+(\vec{r})$ and the electron wave function. Unfortunately it is not possible to decompose $B^{2\gamma}(\vec{r})$ into $B^+(\vec{r})$, the positron part and $B^-(\vec{r})$, the electron part [3] in a straightforward manner.

Schülke [5] has discussed some important theorems for the FTMD which can be applied for examining the effect of solid state properties on FTMD in a transition metal like V. In the case of periodic systems (like the crystalline solids) containing Bloch states, $u_{\vec{k},j}(\vec{r})$, for the electron (having a wave vector $\vec{k}$ and band index j) one can write [3, 5]

$$B^{CP}(\vec{r}) \propto \sum_{j,k} n_j(\vec{k}) \exp[-i\vec{k}\cdot\vec{r}] \int d\vec{s}\, u_{\vec{k},j}^*(\vec{r}+\vec{s})\, u_{\vec{k},j}(\vec{s}) \tag{7}$$

and

$$B^{2\gamma}(\vec{r}) \propto \sum_{j,k} n_j(\vec{k}) \exp[-i\vec{k}\cdot\vec{r}] \int d\vec{s}\, u^{+*}(\vec{r}+\vec{s})\, u_{\vec{k},j}^*(\vec{r}+\vec{s})\, u^+(\vec{s})\, u_{\vec{k},j}(\vec{s}) \tag{8}$$

where $n_j(\vec{k})$ is the occupation number of the Bloch states and $n_j(\vec{k}) = 1$ for occupied states and $n_j(\vec{k}) = 0$ for unoccupied states.

Using these relations Schülke [5] has proved that if $\vec{R}_i$ is a translation vector of the lattice then

i) $$B^{CP}(\vec{r} = \vec{R}_i) = 0 \tag{9}$$

in the case of insulators (completely occupied bands) and

ii) $$B^{CP}(\vec{r} = \vec{R}_i) = (2\pi)^{-3/2} \sum_{j,k} n_j(\vec{k}) \exp[-i\vec{k}\cdot\vec{R}_i] \tag{10}$$

in case of metals (one or more bands partially occupied). In insulators as well as in metals $B^{CP}(\vec{r}=0) \neq 0$ and the value $B(0)$ is used to normalize $B(\vec{r})$.

Inverting equation (10) one has the relation [3, 5]

$$\sum_j n_j(\vec{k}) = \text{Const.} \sum_{\vec{R}_i} B(\vec{R}_i) \exp[i\vec{k}\cdot\vec{R}_i] \tag{11}$$

which show that the values of $B(\vec{r})$ at a translational lattice vector $\vec{r} = \vec{R}_i$ can lead to the determination of the FS of metals.

3. Calculations

The set of experimental $B(\vec{r})$ curves were calculated with the help of equations (3) and (5). The CP data, $J(p_z)$, for V were taken from the work of

Rollason et al. [9], while the 2D-ACPAR data for V are those measured by Manuel et al. [13]. The $B(\vec{r})$ curves derived from experimental CP data were calculated for the three symmetry directions [100], [110] and [111]. They will be denoted by $B^{CP}_{exp}(\vec{r})$. The $B(\vec{r})$ curves calculated from the experimental 2D-ACPAR curves will be denoted by $B^{2\gamma}_{exp}(\vec{r})$. These were obtained along the seven symmetry directions: [100], [110], [111], [120], [121], [221] and [321] by making use of the $N(p_y, p_z)$ surface measured for the four orientations (p_x): [100], [110], [111] and [112]. Some of the $\vec{r}$-directions turned out to be common when all these four orientations were used. It was found that the $B^{2\gamma}_{exp}(\vec{r})$ along the common directions were the same although they were calculated from independent data set for different orientations.

The same electron wave functions were used to calculate theoretical $\rho(\vec{p})$ and $\rho^{2\gamma}(\vec{p})$ by using the LMTO band method [17] as described by Singh and Jarlborg [14]. For these calculations the $\vec{p}$-space was divided into small cubes having an edge size of 0.0549 a.u. and the $\rho(\vec{p})$ and $\rho^{2\gamma}(\vec{p})$, were computed at the corners of such cubes, using about 25 000 $\vec{p}$-points in the $\frac{1}{48}$th irreducible part of $\vec{p}$-space. The FTMD were then calculated with the help of equations (1) and (4). They will be denoted by $B^{CP}_{LMTO}(\vec{r})$ and $B^{2\gamma}_{LMTO}(\vec{r})$ for the case of CP and ACPAR respectively.

In order to compare the experimental $B^{2\gamma}_{exp}(\vec{r})$ with more than one theory, we also caclulated the FTMD from the TPMD obtained by Singh and Singru [15] who had used the band structure method due to Hubbard and Mijnarends [18]. This second set of theoretical $B^{2\gamma}(\vec{r})$ curves will be denoted by $B^{2\gamma}_{HM}(\vec{r})$.

It should be pointed out that both the theoretical calculations [14, 15] of $\rho^{2\gamma}(\vec{p})$ used here were done in IPM which did not include the $e^+ - e^-$ many-body correlations effects. They did include, however, the effects of positron wave function and the contributions from the core electrons.

In order to compare the CP and 2γ FTMD functions on the same basis, the experimental $B(\vec{r})$ functions were deconvoluted with their respective experimental resolution functions. These were assumed to be Gaussians with a FWHM of 0.40 and 0.03 a.u. for the CP data and 2D-ACPAR data. Secondly all the five curves $B^{CP}_{exp}(\vec{r})$, $B^{CP}_{LMTO}(\vec{r})$, $B^{2\gamma}_{exp}(\vec{r})$, $B^{2\gamma}_{LMTO}(\vec{r})$ and $B^{2\gamma}_{HM}(\vec{r})$ were normalized to unity at $\vec{r} = 0$ because of the uncertainty in the normalization of $B^{2\gamma}(\vec{r})$.

4. Results and discussion

4.1. *The $B(\vec{r})$ functions for Compton profile and positron annihilation*

The sets of $B(\vec{r})$ functions we have obtained in V are shown in Figs. 1–7 for the seven directions [100], [110], [111], [120], [121], [221] and [231]. Our results for $B^{CP}_{exp}(\vec{r})$ along the [100], [110] and [111] directions show excellent agreement with those reported by Rollason et al. [9]. In particular the positions, r_0 of the first zeros of the $B^{CP}_{exp}(\vec{r})$ were calculated by us at $r_0 = 3.5$ and 4.3 a.u. along [100] and [111] respectively and they agree with the values of $r_0 = 3.5$ and 4.25 a.u. observed by Rollason et al. [9]. The values of r_0 obtained by us for the different $B(\vec{r})$ functions and by other workers for different directions are summarized in Table 1. The values of r_0 calculated from the LMTO theory are in closer agreement with experiment [9] than those calculated from the LCAO theory [19].

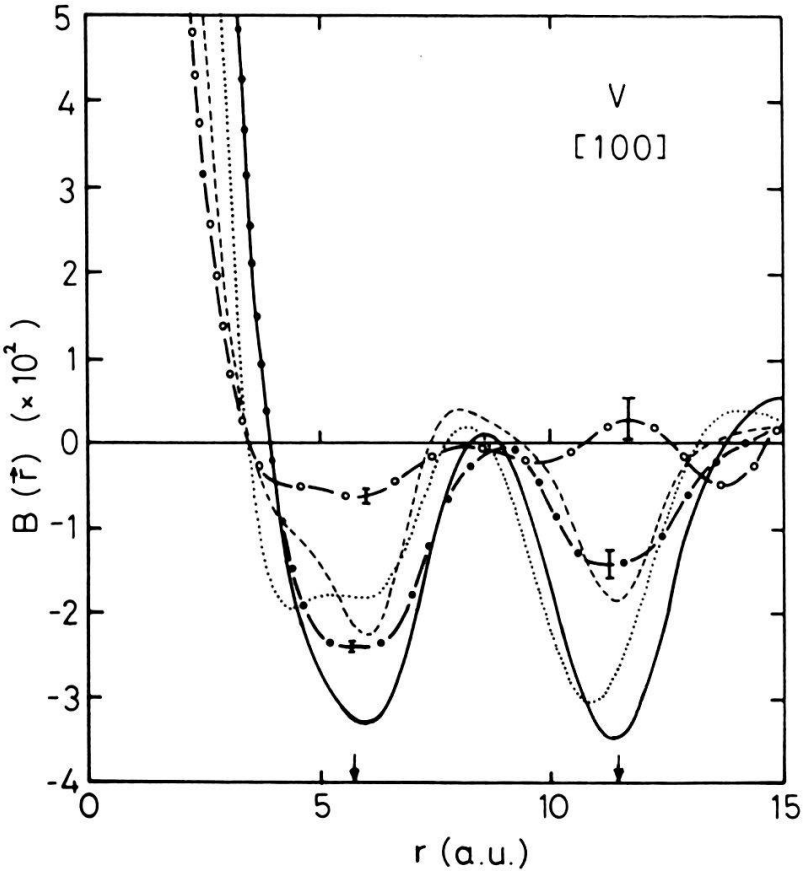

Figure 1
The Fourier transform of the momentum density in the [100] direction of V. $B^{CP}_{exp}(\vec{r})$, $B^{CP}_{LMTO}(\vec{r})$, $B^{2\gamma}_{exp}(\vec{r})$, $B^{2\gamma}_{LMTO}(\vec{r})$ and $B^{2\gamma}_{HM}(\vec{r})$ are represented by (-○-○-), (- - - - -), (-●-●-), (———) and (·····) respectively. The vertical scale gives the values of $B(\vec{r})$ after normalizing them equal to one at $\vec{r} = 0$. Error bars are shown for the experimental Curves.

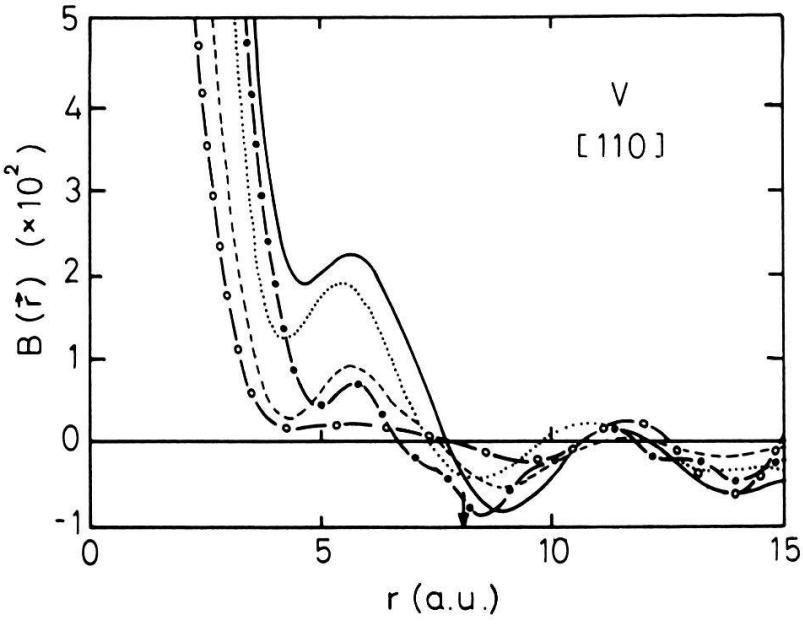

Figure 2
Same as for Figure 1 but for the direction [110].

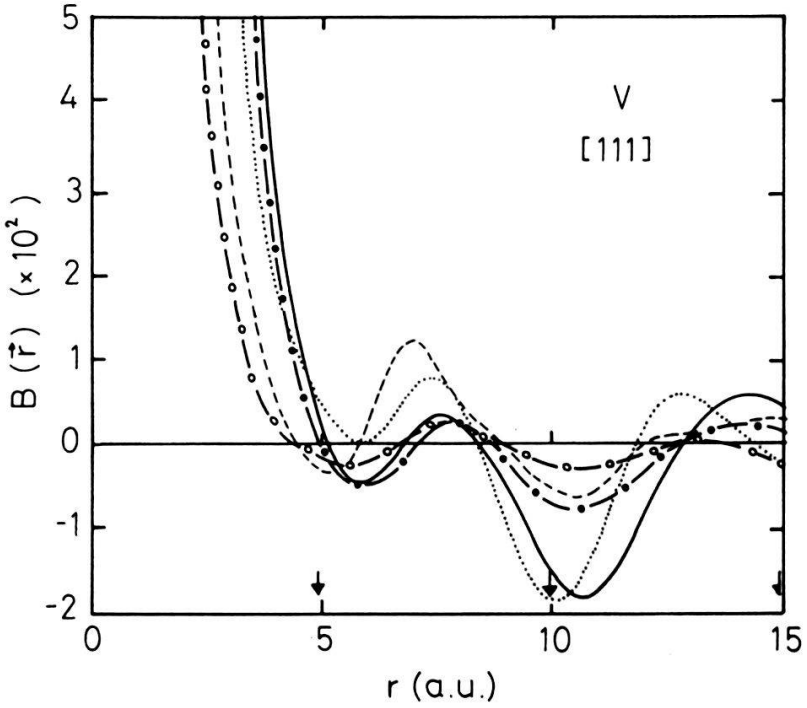

Figure 3
Same as for Figure 1 but for the direction [111].

It will be useful to discuss some common features seen in the different $B(\vec{r})$ functions of Figs. 1–7 before discussing their characteristic behaviour along a particular direction. Firstly in the absence of any experimental data for the CP along the last four directions (Table 1) we could not present the $B^{CP}_{exp}(\vec{r})$ curves in Figs. 4–7. An overall examination of each of the $B(\vec{r})$ curves along the seven directions indicate their strong anisotropy in the $\vec{r}$-space. This anisotropy arises from the anisotropy of the FS and the anisotropies in the electron and positron wave functions. The charge asphericity in metallic V is known to be strong and has been studied by various workers [20]. The X-ray form factors for V have been analyzed

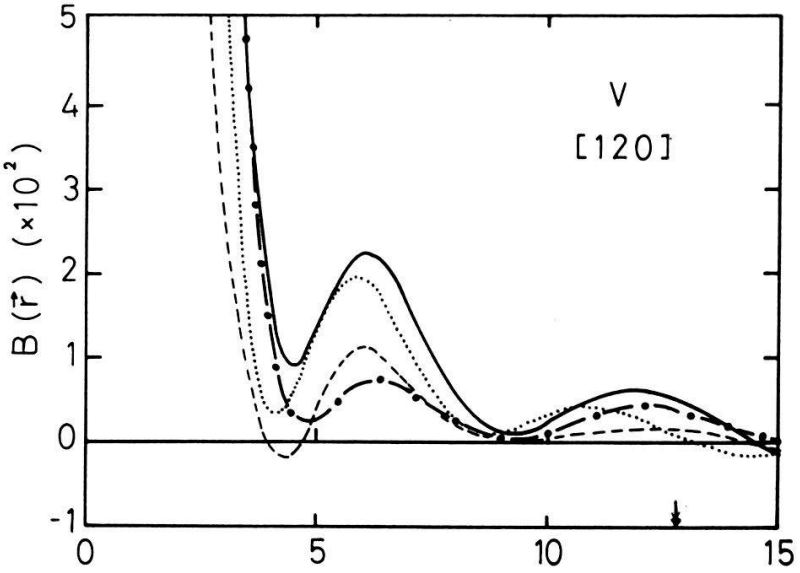

Figure 4
Same as for Figure 1 but for the direction [120]. The $B^{CP}_{exp}(\vec{r})$ curves are not shown.

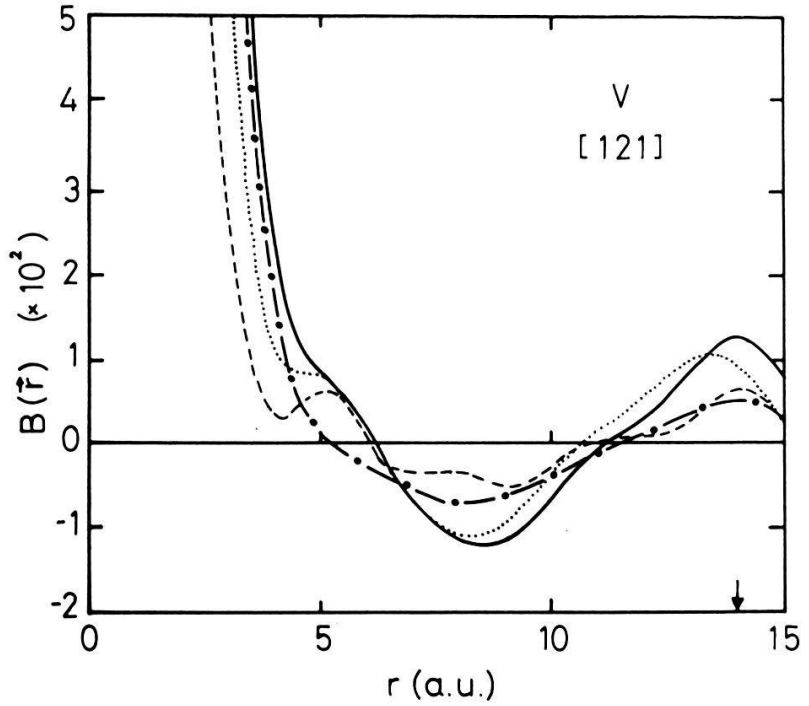

Figure 5
Same as for Figure 4 but for the direction [121].

in terms of the E_g and T_{2g} orbitals. Since the charge density, $\rho(\vec{r})$, and the autocorrelation function, $B(\vec{r})$, arise both from the electron wave function $\psi(\vec{r})$, the anisotropy in $B(\vec{r})$ and $\rho(\vec{r})$ is interrelated.

In view of the theorems described by equations (9) and (10) it will be important to examine the behaviour of the different $B(\vec{r})$ functions near $\vec{r} = \vec{R}_i$, the translation vectors of the lattice. To facilitate such an examination we have

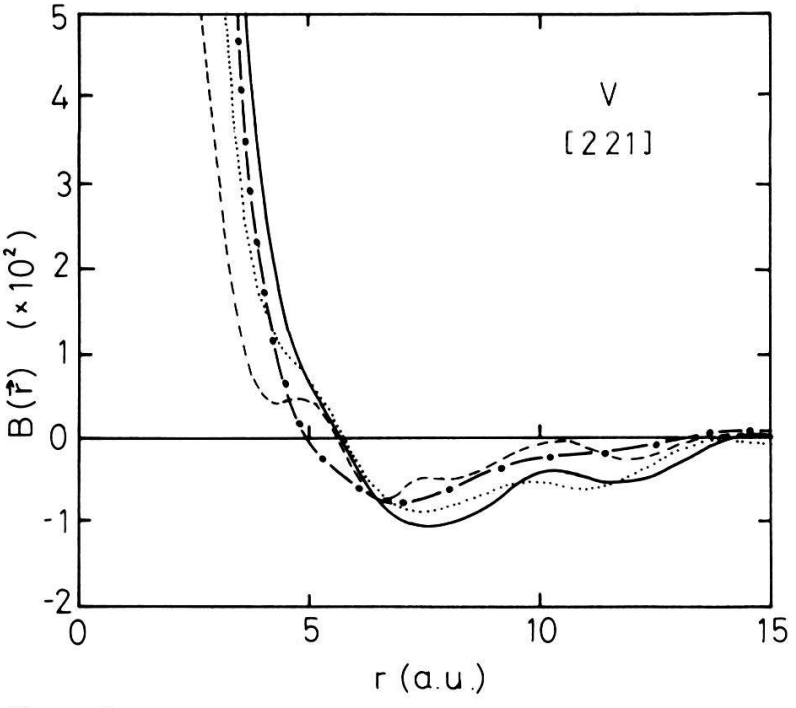

Figure 6
Same as for Figure 4 but for the direction [221].

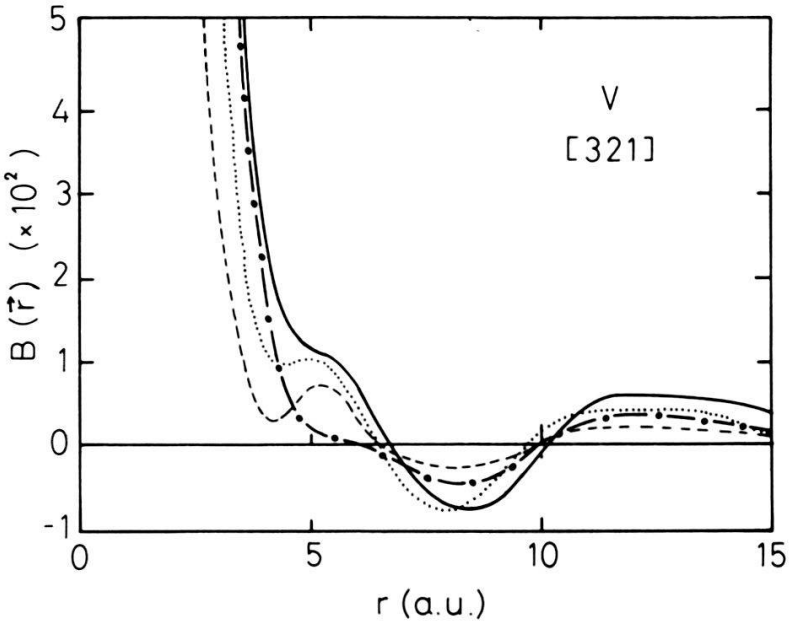

Figure 7
Same as for Figure 4 but for the direction [321].

given the values of $\vec{R}_i$ for the seven directions in Table 2. It should be remembered that the $B(\vec{r})$ functions shown in Figs. 1–7 are the one dimensional projections, $B(z)$, and the effect of other directions projected onto z should also be considered while examining the $B(\vec{r})$ curves [11]. Keeping this in mind, we have indicated the projected values of $\vec{R}_i$ in Table 2. The $\vec{r} = \vec{R}_i$ are shown by vertical arrows in Figs. 1–7. The results of Figures 1–7 indicate, as expected for a

Table 1
Position of the first zeros (r_0) in a.u. for the different $B(\vec{r})$ functions in V along various directions.

	Direction						
Function	[100]	[110]	[111]	[120]	[121]	[221]	[321]
$B^{CP}_{exp}(\vec{r})^{(a)}$	3.5	7.5	4.25	—	—	—	—
$B^{CP}_{exp}(\vec{r})^{(b)}$	3.5	7.9	4.30	—	—	—	—
$B^{CP}_{LMTO}(\vec{r})^{(c)}$	3.5	7.5	4.3	3.9	6.1	5.5	6.5
$B^{CP}_{LCAO}(\vec{r})^{(d)}$	3.45	7.33	4.55	—	—	—	—
$B^{2\gamma}_{exp}(\vec{r})^{(e)}$	3.9	6.7	4.9	15.3	5.3	4.9	5.9
$B^{2\gamma}_{LMTO}(\vec{r})^{(c)}$	3.9	7.7	5.1	14.3	6.1	5.9	6.7
$B^{2\gamma}_{HM}(\vec{r})^{(f)}$	3.5	7.3	8.3	13.1	6.1	5.7	6.5

a) Reference [9].
b) Present work based on the experimental CP [9].
c) Present work based on LMTO band structure method.
d) Reference [9] based on LCAO method [19].
e) Present work based on the 2D-ACPAR experiment [13]
f) Present work based on Hubbard–Mijnarends method [15].

Table 2
Lattice translation vectors, $\vec{R}_i$ in the position space for V along different symmetry directions. The value of the lattice parameter, $a = 5.726$ a.u. (used in LMTO calculations) is taken at present

Direction	$r = R_i$ in a.u. at integer multiple of	Projections from other directions in a.u. at integer multiple of
[100]	$a = 5.726$	$(a/2) = 2.863$
[110]	$(a\sqrt{2}) = 8.098$	$(a/\sqrt{2}) = 4.049$
[111]	$(a\sqrt{3}/2) = 4.959$	$(a/2\sqrt{3}) = 1.653$
[120]	$(a\sqrt{5}) = 12.804$	$(a/2\sqrt{5}) = 1.280$
[121]	$(a\sqrt{6}) = 14.026$	$(a/\sqrt{6}) = 2.338$
[221]	$3a = 17.178$	$(a/6) = 0.954$
[321]	$(a\sqrt{14}) = 21.425$	$(a/\sqrt{14}) = 1.530$

metal, that different $B(\vec{r})$ functions do not cross through zero at $\vec{r} = \vec{R}_i$ but they have a sizable value, and in some cases interesting structure, around $\vec{r} = \vec{R}_i$. Similar behaviour of the $B(\vec{r})$ functions was observed for V [9], Fe [11] and Cu [12]. In this regard it is useful to recall that Pattison et al. [12] have written an approximate relation for $B(\vec{r})$ due to a given band as

$$B(\vec{r}) = B_S(\vec{r})B_u(\vec{r}) \tag{12}$$

where $B_S(\vec{r})$ is the part determined by the shape of the FS and $B_u(\vec{r})$ is the determined band autocorrelation function of the periodic part of the Bloch wave functions. In the case of a metal like V, a filled band will have $B_S(\vec{r}) = 0$ at $\vec{r} = \vec{R}_i$ and the contribution from $B_u(\vec{r})$ due to filled band will be thus suppressed at $\vec{r} = \vec{R}_i$. The contribution to $B(\vec{r})$ at $\vec{r} = \vec{R}_i$ from a partially filled band (like in V) will come from $B_S(\vec{r})$ (i.e. FS topology) as well as $B_u(\vec{r})$ (i.e. band average periodic functions).

Although $B^{2\gamma}(\vec{r})$ for Al [3, 21], $Mg_{70}Zn_{30}$ [22] and V_3Si [3, 23] have been reported, there is no report of $B^{2\gamma}(\vec{r})$ in a transition metal in the literature, as far as we know. From this point of view, the $B^{2\gamma}_{exp}(\vec{r})$ functions for V (Figs. 1–7) and their comparison with $B^{CP}(\vec{r})$ and $B^{2\gamma}_{LMTO}(\vec{r})$, $B^{2\gamma}_{HM}(\vec{r})$ provide novel information. One can notice the similar shapes displayed by $B^{CP}(\vec{r})$ and $B^{2\gamma}(\vec{r})$ functions specially in the region $r < 10.0$ a.u. These two functions appear to be shifted along $\vec{r}$-axis and these shifts could be ascribed partly to the radial behaviour of the positron wave function in V [15] which is shown in Fig. 8. The net difference in the $B^{CP}_{exp}(\vec{r})$ and $B^{2\gamma}_{exp}(\vec{r})$ curves are attributed to the combined effects of the positron wave function and $e^+ - e^-$ correlations. These two effects bring further anisotropy in $B^{2\gamma}(\vec{r})$ as will be discussed later on. The $B^{2\gamma}(\vec{r})$ curves show larger values at large $\vec{r}$-values. This is due to the large amplitude of the positron wave function in the interstitial region. The tails of the $B^{2\gamma}(\vec{r})$ functions appear to persist beyond $r > 15$ a.u. whereas the $B^{CP}(\vec{r})$ die out in this region. This behaviour is due to the fact that $\rho^{2\gamma}(\vec{p}) > \rho^{CP}(\vec{p})$ at low ($p > 2.0$ a.u.) momenta, resulting from the increased role played by valence electrons in ACPAR.

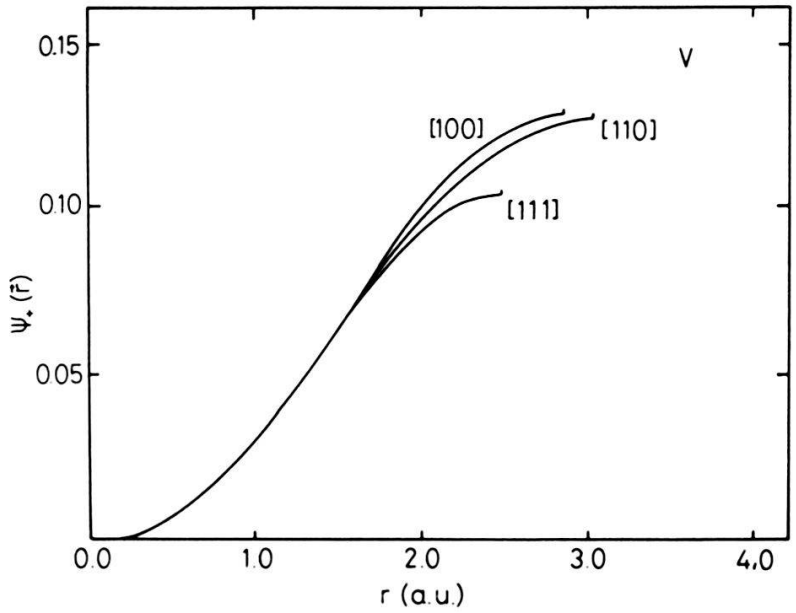

Figure 8
The plot of the positron wave function $\psi_+(\vec{r})$ in V along the directions [100], [110] and [111].

It may be noted that the $B^{2\gamma}(\vec{r})$ curves in Figs. 1, 5, 6 and 7 are smoother compared to the corresponding $B^{CP}(\vec{r})$ curves in the region $r = 5$–10 a.u. We ascribe this behaviour to the nature of the positron wave function shown in Fig. 8. In the case of ACPAR, the $B_S(\vec{r})$ function defined in equation (12) remains unchanged (as for CP) while $B_u(\vec{r})$ is modified by the positron wave function. The low valued and isotropic nature of the positron wave function for $r < 2.0$ a.u. may damp out structures in $B_u(\vec{r})$ i.e. the periodic part of the autocorrelation function, contributed by the electron wave functions.

We shall now discuss the results for the different $B(\vec{r})$ functions along each direction separately.

a) [100] direction:

Although the position of the first zero r_0 does not occur at $\vec{r} = \vec{R}_{100} = 5.726$ a.u. (Table 2) for any of $B(\vec{r})$ curves in Fig. 1, there is an agreement between the values of r_0 for $B^{CP}_{exp}(\vec{r})$ and $B^{CP}_{LMTO}(\vec{r})$ and for $B^{2\gamma}_{exp}(\vec{r})$ and $B^{2\gamma}_{LMTO}(\vec{r})$ (Table 1). In the case of $B^{2\gamma}_{HM}(\vec{r})$ we observe $r_0 = 3.5$ a.u. which is to left of the r_0-value of the other two $B^{2\gamma}(\vec{r})$ curves. Each of the $B(\vec{r})$ curve in Fig. 1 show a deep minima (accompanied by a structure in some cases) around $\vec{r} = \vec{R}_{100} = 5.726$ and $\vec{r} = \vec{R}_{200} = 11.452$ a.u. Similar behaviour was observed for $B^{CP}_{exp}(\vec{r})$ in V [9], Fe [11] and Cu [12] along the [100] directions. Following the discussion of equation (12) given by Pattison et al. [12], it is suggested that the magnitudes of $B(\vec{R}_{100})$ and $B(\vec{R}_{200})$ are built from the contributions from the FS as well as the autocorrelation functions. The differences in the shapes (and sizes) of $B^{CP}_{exp}(\vec{r})$ and $B^{2\gamma}_{exp}(\vec{r})$ are due to the effects of positron wave function (Fig. 8) and $e^+ - e^-$ many-body correlations. In the case of Al, Berko et al. [21] have found that the $e^+ - e^-$ many-body effect, when described by the Kahana's [24] enhancement formula, changes the position of r_0 (first zero crossing) as well as the values of $B^{2\gamma}(\vec{r})$ at other $r > r_0$. In 3d transition metals the $e^+ - e^-$ many-body effects might not be described by a momentum-dependent enhancement formula [24] but a more complex energy-dependent formula, as found for Fe [25] and Cu [26]. We plan to

apply such an enhancement correction as a part of our future work on V. Consequently, we shall not elaborate this aspect of discussion at this stage.

It appears from Fig. 1 that $B^{2\gamma}_{exp}(\vec{r})$, $B^{2\gamma}_{LMTO}(\vec{r})$ and $B^{2\gamma}_{HM}(\vec{r})$ show similar shapes although their radial dependence do not overlap. The differences between $B^{2\gamma}_{LMTO}(\vec{r})$ and $B^{2\gamma}_{HM}(\vec{r})$ are attributed to the fact that the electron and positron wave functions, as well as some other computational details used in the calculation of these two functions, are different [14, 15]. The observed differences, however, emphasize the fact that the FTMD, $B^{2\gamma}(\vec{r})$, are more sensitive to the differences in the band structure calculations than what $N(p_y, p_z)$ surfaces might reveal. One can notice that the $B^{2\gamma}_{LMTO}(\vec{r})$ show better agreement with $B^{2\gamma}_{exp}(\vec{r})$ than $B^{2\gamma}_{HM}(\vec{r})$ at present. But it must be remembered that the potential for the positron, in the case of $B^{2\gamma}_{HM}(\vec{r})$, was the same as that for the electron but with negative sign. However, the exchange part was also taken out in the case of $B^{2\gamma}_{LMTO}(\vec{r})$. The lattice constant used in these two calculations were also different. Also the differences between the experimental and theoretical $B^{2\gamma}(\vec{r})$ functions are caused by the omission of the $e^+ - e^-$ many body effects in both theories. Therefore, no final judgement about the better agreement of a particular theory with experiment can be expressed until $e^+ - e^-$ many-body corrections are properly included in the theories.

b) [110] direction:

An interesting feature of the $B(\vec{r})$ functions (Fig. 2) along the [110] direction is the appearance of the 'shoulder' or a minimum followed by a maximum before the function passes through a zero. The minima and maxima occur in the range $r = 4.2$–5.0 and $r = 5.4$–5.8 respectively and thus the onset of the shoulder structure is immediately after $r = a/\sqrt{2} = 4.05$ a.u. where the [100] and $[\frac{1}{2}, \frac{1}{2}, \frac{1}{2}]$ vectors get projected onto the [110] direction (Table 2). This behaviour indicates interesting interplay between the effects of FS and autocorrelation functions (equation (12)) in the range $r = 4.0$–6.0 a.u. The structure in the 'shoulder' is smoother in $B^{CP}_{exp}(\vec{r})$ compared to other $B(\vec{r})$ curves shown in Fig. 2. A shoulder-like structure at $r = a/\sqrt{2} = 4.05$ a.u. was also observed in the $B^{CP}(\vec{r})$ functions for Fe [11] and Cu [12]. Another interesting feature of the $B(\vec{r})$ curves in Fig. 2 is that their first zeros (r_0) occur close to $\vec{r} = \vec{R}_{110} = 8.10$ a.u. (Table 1 and 2). Similar behaviour is observed for Fe [11] along the [110] direction. Other interesting features displayed by different $B(\vec{r})$ functions in Fig. 2 can be understood in a manner similar to that in a previous discussion of the results for the [100] direction.

c) [111] direction:

Different $B(\vec{r})$ curves in Fig. 3 show shapes similar to each other and to those in Fig. 1, but are different from $B^{CP}_{exp}(\vec{r})$ observed for Fe [11] along the [111] direction. Minima in the curves $B^{CP}_{exp}(\vec{r})$ and $B^{CP}_{LMTO}(\vec{r})$ occur nearer $r = (a\sqrt{3}/2) = 4.96$ a.u. the interatomic distance, than the minima in the $B^{2\gamma}_{exp}(\vec{r})$ and $B^{2\gamma}_{LMTO}(\vec{r})$ curves (Fig. 3). The shift between the $B^{CP}(\vec{r})$ and $B^{2\gamma}(\vec{r})$ is ascribed to the effects of positron as discussed above. The narrow minima and maxima observed in the shapes of the $B(\vec{r})$ curves for the [100] (Fig. 1) and [111] (Fig. 3) directions could be ascribed to the effects of the localized nature of the d-electrons (having energies near the Fermi energy E_F) on the $B_u(\vec{r})$ functions [12].

d) Other directions:

The results of different $B(\vec{r})$ functions for the other four directions (Figs. 4–7) can be discussed in a similar manner and we shall not go into it. The functions

$B^{CP}_{exp}(\vec{r})$ along these four directions are not available owing to the lack of experimental data and we suggest that CP along these directions should be experimentally measured to provide $B^{CP}_{exp}(\vec{r})$ which can be compared with the theoretical curves $B^{CP}_{LMTO}(\vec{r})$ shown in Figs. 4–7.

4.2. *Differences between the CP and 2γ $B(\vec{r})$ functions*

We have evaluated two types of difference curves

$$\Delta B_{exp}(\vec{r}) = B^{2\gamma}_{exp}(\vec{r}) - B^{CP}_{exp}(\vec{r}) \tag{13}$$

$$\Delta B_{th}(\vec{r}) = B^{2\gamma}_{LMTO}(\vec{r}) - B^{CP}_{LMTO}(\vec{r}) \tag{14}$$

with an aim to bring out the effects of positron wave function and $e^+ - e^-$ many-body correlations more sensitively. These difference curves for the $\vec{r}$-directions [100], [110] and [111] are plotted in Figs. 9–11 respectively and they show interesting behaviour. The radial dependence of the $\Delta B_{exp}(\vec{r})$ is expected to show the effects of positron wave function as well as $e^+ - e^-$ many-body correla-

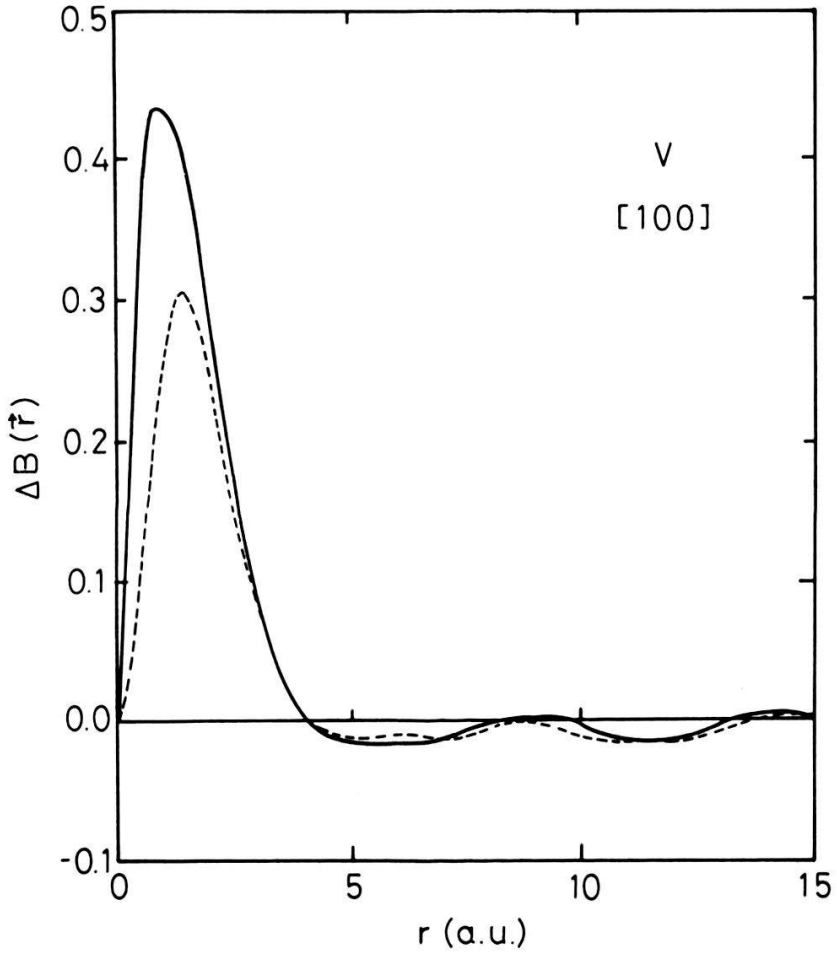

Figure 9
Differences between positron and Compton $B(\vec{r})$ functions, along the [100] direction in V. (———) is the experimental difference while (– – – –) is the difference obtained with the LMTO band structure calculation.

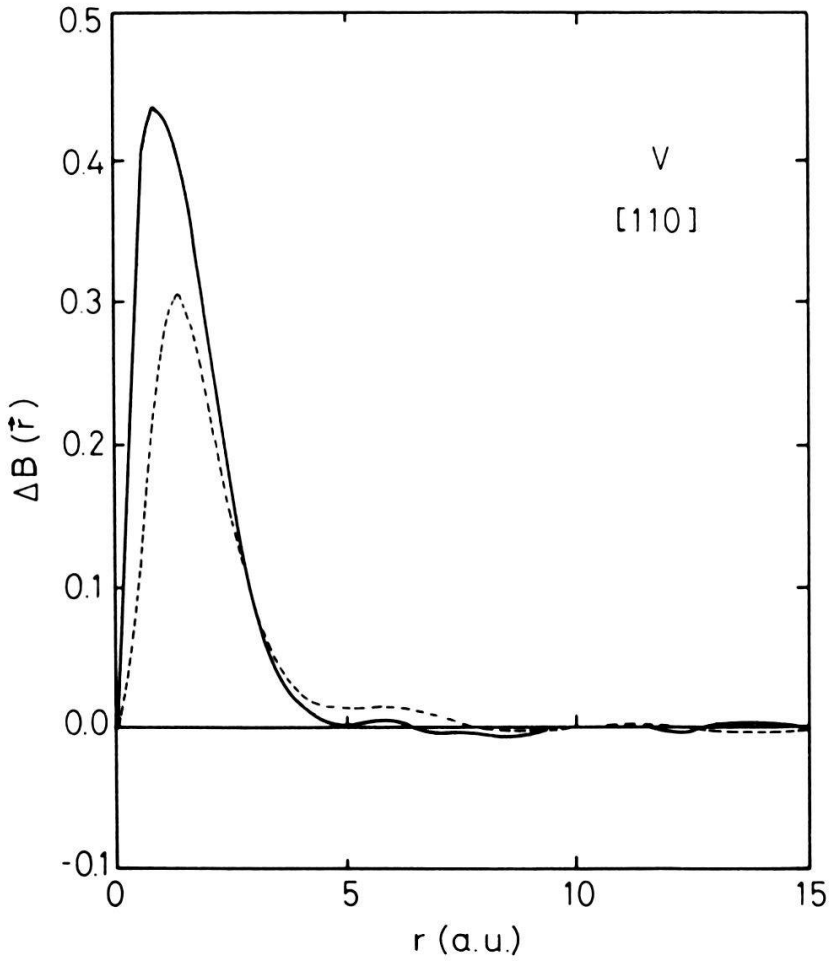

Figure 10
Same as for Figure 8 but for the direction [110].

tions while that of $\Delta B_{\text{th}}(\vec{r})$ will show the effects of positron wave function which was already taken into account while calculating $B^{2\gamma}_{\text{LMTO}}(\vec{r})$.

Both $\Delta B_{\text{exp}}(\vec{r})$ and $\Delta B_{\text{th}}(\vec{r})$ display sharp, narrow and positive peaks at low ($r < 4.0$ a.u.) r-values, followed by relatively weak but anisotropic oscillations in the range $r = 4$–12 a.u. The peaks in the $\Delta B_{\text{exp}}(\vec{r})$ and $\Delta B_{\text{th}}(\vec{r})$ are centered around $r = 0.9$ a.u. and 1.4 a.u. respectively with a FWHM of about 2.0 a.u. for each. Weyrich et al. [6] have reported how the different (n, l) atomic orbitals contribute to $B^{\text{CP}}(\vec{r})$ in Krypton. These results can provide us with some guidance. Even though we are interested in V having configuration (Argon)$(3d)^3(4s)^2$ and one should expect the core electron contributions to $B(\vec{r})$ to play a major role at low $\vec{r}$-values ($r < 1.0$ a.u.) and balance electrons to contribute at higher $\vec{r}$-values. The common $\vec{r}$-dependence of $\Delta B_{\text{exp}}(\vec{r})$ and $\Delta B_{\text{th}}(\vec{r})$ is, therefore, ascribed to the overlap of positron and electron wave functions which is different for core and valence electrons. The differences between $\Delta B_{\text{exp}}(\vec{r})$ and $\Delta B_{\text{th}}(\vec{r})$ are sharper at low ($r < 1.0$ a.u.) r-values than at large ($r > 4.0$ a.u.) r-values, and they indicate that the $e^+ - e^-$ many-body correlations effects are different for core and band electrons. Similar explanation has been proposed elsewhere [2, 3, 26]. The present results in Figs. 9–11 indicate further that $e^+ - e^-$ many-body correlations effects for core as well as band electrons are anisotropic.

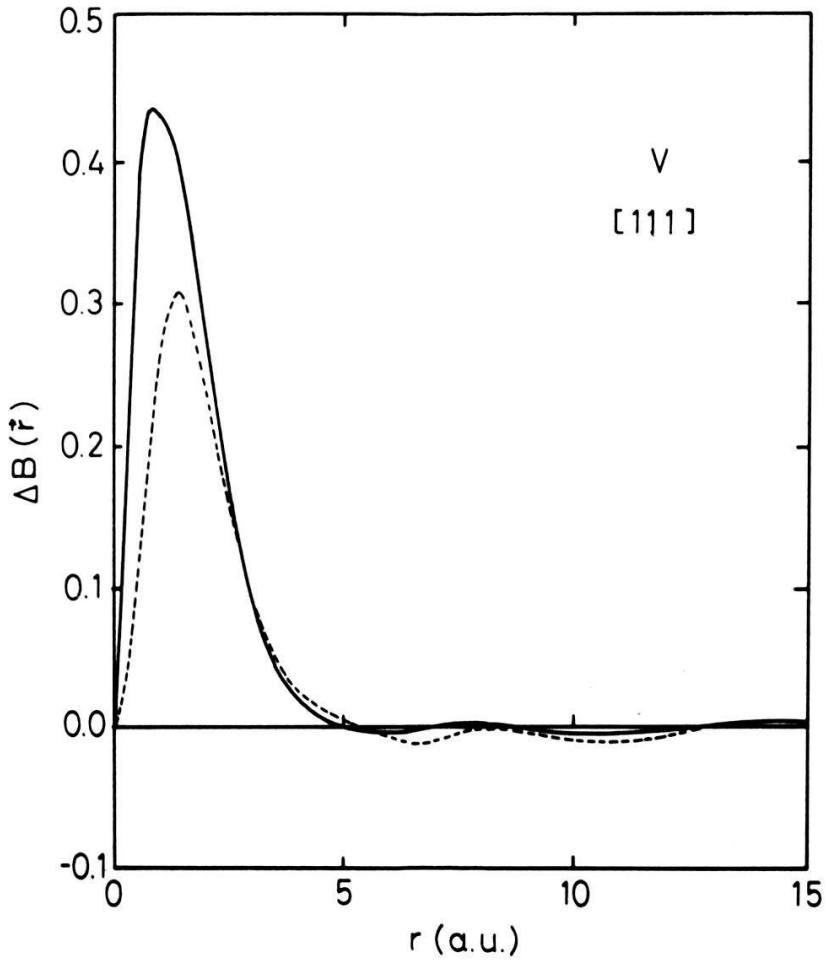

Figure 11
Same as for Figure 9 but for the direction [111].

4.3. *Anistropy profiles*

In order to bring out the anisotropic effects of the many-body correlations, we have evaluated profiles of anisotropy defined by

$$A^1_{\text{exp}}(r) = \Delta B_{\text{exp}}(\vec{r} = [110]) - \Delta B_{\text{exp}}(\vec{r} = [100]) \tag{15}$$

and

$$A^1_{\text{th}}(r) = \Delta B_{\text{th}}(\vec{r} = [110]) - \Delta B_{\text{th}}(\vec{r} = [100]) \tag{16}$$

for the [110]–[100] directions. Similarly, we have calculated $A^2(r)$ and $A^3(r)$ profiles of anisotropy, for [111]–[110] and [100]–[111] respectively. These anisotropy profiles are shown in Figs. 12–14. It should be remembered that $A^i_{\text{exp}}(r)$ ($i = 1, 2, 3$) describe the effects of positron wave function as well as $e^+ - e^-$ many-body correlations while $A^i_{\text{th}}(r)$ contain only the effects of positron wave function. In spite of this, the general shape of the $A(r)$ profiles in the region $r > 3.0$ a.u. is surprisingly similar for all the three sets of directions. This behaviour suggests that the anisotropy in the $\Delta B(\vec{r})$ curves is determined mainly by the effects of positron wave function, while the magnitude of the anisotropy is affected by the $e^+ - e^-$ many-body correlations. The differences between $A^i_{\text{exp}}(r)$ and $A^i_{\text{th}}(r)$ observed (Figs. 12–14) may not be explained so easily unless one

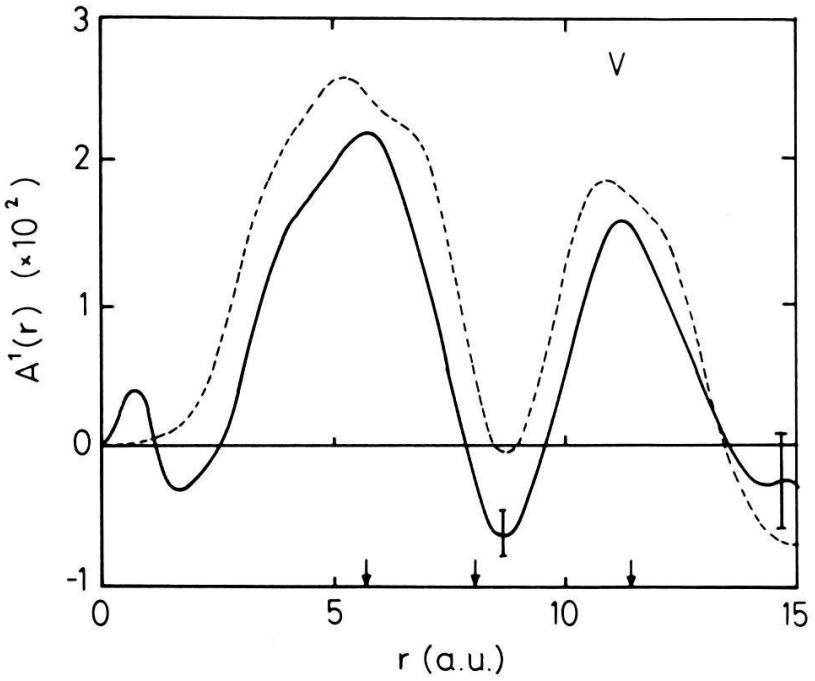

Figure 12
The anisotropies $A^1_{exp}(r)$ and $A^1_{th}(r)$ (see text) are shown by (———) and (- - - -) respectively.

understands properly the effects of propagation of experimental errors (inherent at large momentum values) into the small r-values ($r < 3.0$ a.u.). An interesting observation we wish to make finally is that the maxima and minima observed in the $A^i_{exp}(r)$ and $A^i_{th}(r)$ occur around the same r-values which in some cases to be $\vec{r} = \vec{R}_i$ (Table 2) as shown by the vertical arrows in Figs. 12–14.

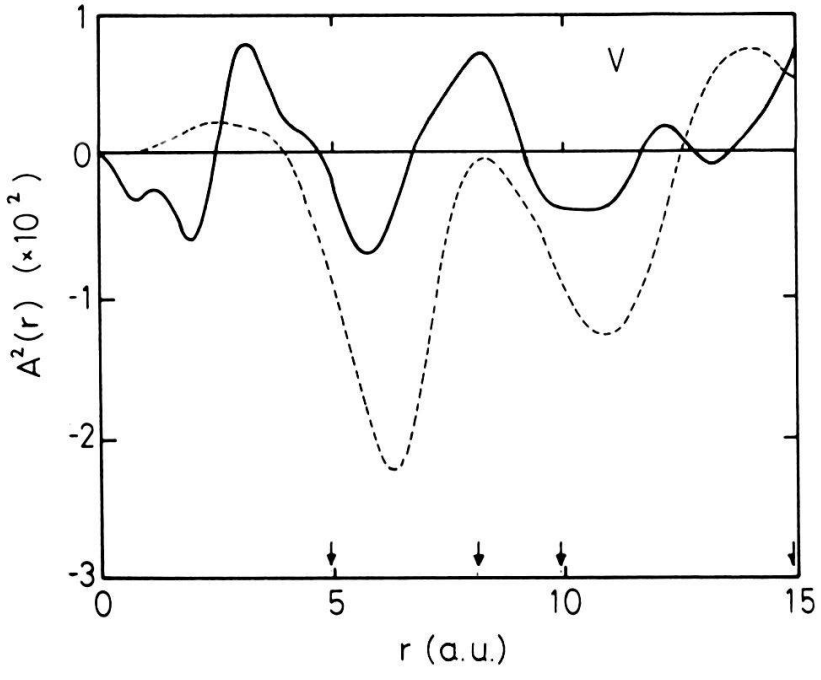

Figure 13
Same as for Figure 11 but for anisotropies $A^2_{exp}(r)$ and $A^2_{th}(r)$.

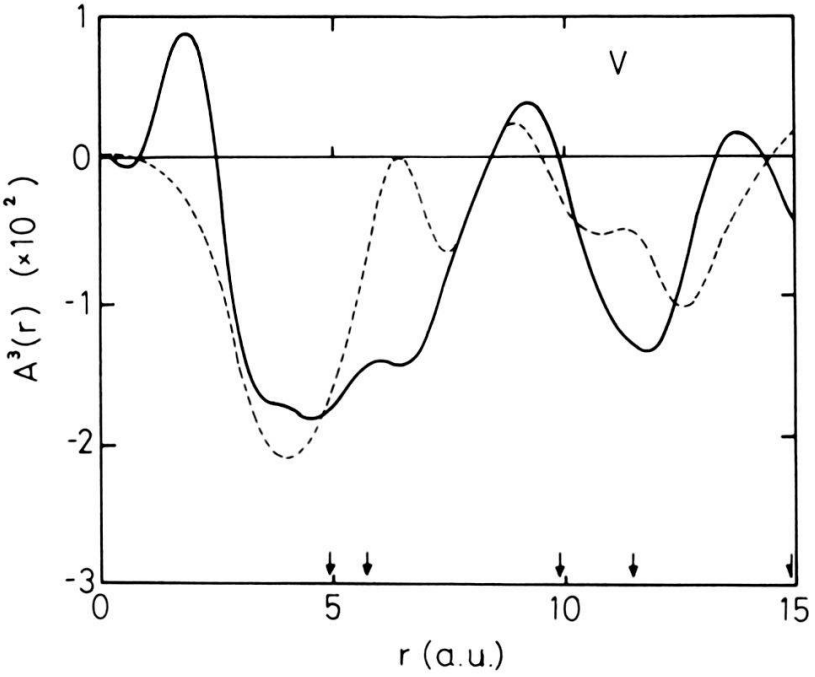

Figure 14
Same as for Figure 11 but for anisotropies $A^3_{exp}(r)$ and $A^3_{th}(r)$.

5. Conclusions

The FTMD, $B(\vec{r})$, for different $\vec{r}$-directions in V has been derived from the experimental and theoretical CP and ACPAR results. These results show that each of the $B(\vec{r})$ function is anisotropic in the position space. The $B(\vec{r})$ functions in V show finite values at the lattice translation vectors $\vec{r} = \vec{R}_i$, their magnitude being determined by the Fermi surface topology and the nature of the wave functions. The effects of positron wave function and $e^+ - e^-$ many-body correlations are observed from the differences in the $B(\vec{r})$ functions for CP and ACPAR. Further, the $B(\vec{r})$ function is sensitive to the differences in the electron (and positron) wave functions (and hence the band structure method) used. The anisotropic nature of the positron wave function introduces anisotropy in the $B^{2\gamma}(\vec{r})$ function, which can also be used to examine the different $e^+ - e^-$ many-body correlations contributed by the core and band electrons. On the whole the FTMD $B^{CP}(\vec{r})$ and $B^{2\gamma}(\vec{r})$ are very useful functions to analyze sensitively the CP and ACPAR data.

The reconstruction of the full three-dimensional EMD, $\rho(\vec{p})$ from the 1D CP data and of $\rho^{2\gamma}(\vec{p})$ from the 2D ACPAR data is a challenging problem [2–4]. In view of the fact that the FTMD, $B(\vec{r})$, functions plays an important role in some of these reconstruction techniques [3], the present results can be of interest for the problem of reconstructing momentum densities in V [27, 28]. Similarly the Lock-Crip–West (LCW) theorem [29] has been used to analyze the CP and ACPAR data in metals and its validity for V has been examined by Singh and Singru [30]. There is a close relation between the properties of $B(\vec{r})$ function and the LCW theorem as pointed out by Berko [3]. The results presented above and those obtained in the application of the LCW theorem to V [30] can be combined to understand the relation between the LCW theorem and the properties of $B(\vec{r})$.

Acknowledgement

We are grateful to J. R. Schneider, P. Pattison and R. S. Holt for communicating their results before publication. We thank T. Jarlborg for providing his band structure calculations. This work was partly supported by the Swiss National Science Foundation.

REFERENCES

[1] B. Williams (ed.), *Compton Scattering* (McGraw-Hill, 1977).
[2] P. E. Mijnarends, in *Positrons in Solids*, edited by P. Hautojarvi, (Springer 1979), p. 25–88.
[3] S. Berko, in *Positron Solid-State Physics*, edited by W. Brandt and A. Dupasquier (North-Holland, 1983), p. 64–145.
[4] R. M. Singru, in *Positron Annihilation*, edited by P. G. Coleman, S. C. Sharma and L. M. Diana, (North-Holland, 1982), p. 271–80.
[5] W. Schülke, Phys. Status Solidi (b) *82*, 229 (1977); W. Schülke, Phys. Status Solidi (b) *80*, K67 (1977).
[6] W. Weyrich, P. Pattison and B. G. Williams, Chem. Phys. *41*, 271 (1979).
[7] P. Pattison and J. R. Schneider, Acta Cryst. A*36*, 390 (1980).
[8] P. Pattison, N. K. Hansen and J. R. Schneider, Chem. Phys. *59*, 231 (1981).
[9] A. J. Rollason, R. S. Holt and M. J. Cooper, Phil. Mag. B*47*, 51 (1983).
[10] J. Ashkenazy, private communication.
[11] A. J. Rollason, R. S. Holt and M. J. Copper, J. Phys. F*13*, 1807 (1983).
[12] P. Pattison, N. K. Hansen and J. R. Schneider, Z. Phys. B, Condensed Matter *46*, 285 (1982).
[13] A. A. Manuel, R. Sachot, P. Descouts, M. Peter, R. M. Singru and A. K. Singh, Solid State Commun. *45*, 799 (1983).
[14] A. K. Singh and T. Jarlborg, to appear in J. Phys. F, March 1985.
[15] A. K. Singh and R. M. Singru, J. Phys. F*12*, 685 (1982).
[16] B. Benesch, S. R. Singh and V. H. Smith Jr., Chem. Phys. Lett. *10*, 151 (1971).
[17] O. K. Anderson, Phys. Rev. B*12*, 3060 (1975).
[18] J. Hubbard and P. E. Mijnarends, J. Phys. C*2*, 1222 (1972); P. E. Mijnarends, Physica *63*, 235 (1973).
[19] D. G. Laurent, C. S. Wang and J. Callaway, Phys. Rev. B*17*, 455 (1978).
[20] S. Wakoh and Y. Kubo, J. Phys. F*10*, 2707 (1980) and references cited therein.
[21] S. Berko, W. S. Farmer and F. Sinclair, in *Positron Annihilation* (Proceedings of the Sixth International Conference on Positron Annihilation) edited by P. G. Coleman, S. C. Sharma and L. M. Diani (North-Holland 1982).
[22] N. Shiotani, N. Sakai, H. Sekizawa and T. Mizoguchi, J. Phys. Soc. Jpn, 50, 828 (1981).
[23] S. Berko, W. S. Farmer and F. Sinclair (To be published).
[24] S. Kahana, Phys. Rev. *129*, 1622 (1963); J. P. Carbotte and S. Kahana, ibid. *139*, A213 (1965).
[25] M. Sob, J. Phys. F*12*, 571 (1982).
[27] A. A. Manuel, Phys. Rev. Lett. *49*, 1525 (1982).
[28] L. M. Pecora, A. C. Erhlich, A. A. Manuel, A. K. Singh and R. N. Singru, in proceedings of the 7th International Conference on Positron Annihilation, New-Delhi, 1985.
[29] D. G. Lock, V. H. C. Crip and R. N. West, J. Phys. F*3*, 561 (1973).
[30] A. K. Singh and R. M. Singru, J. Phys. F*14*, 1751 (1984).